Radial basis functions: Developments and applications to planetary scale flows

Natasha Flyer[a,*], Bengt Fornberg[b]

[a] *National Center for Atmospheric Research, Boulder, CO 80305, USA*
[b] *University of Colorado, Department of Applied Mathematics, 526 UCB, Boulder, CO 80309, USA*

Abstract

Radial basis functions (RBFs) can be seen as a major generalization of pseudospectral (PS) methods, abandoning the orthogonality of the basis functions and in return obtaining much improved simplicity and geometric flexibility. Spectral accuracy becomes now easily available also when using completely unstructured node layouts, permitting local node refinements in critical areas. The first major PDE applications for which RBFs have been shown to compete successfully against the best currently available numerical approaches can be found in the geosciences. Examples that are discussed here include translating vortex roll-ups (cyclogenesis), nonlinear flows on the sphere modeled by the shallow water equations, and 3D convection in the earth's mantle.

Keywords: Radial basis functions, RBF, spherical geometry, transport schemes, shallow water equations, mantle convection

*Corresponding Author
Email addresses: flyer@ucar.edu (Natasha Flyer), fornberg@colorado.edu (Bengt Fornberg)

1. Introduction

Radial basis functions (RBFs) were first applied to the task of solving PDEs about 20 years ago [1, 2]. While high accuracy and geometric flexibility have always been noted strengths of the approach [3], it is only in the last few years that their application to PDEs has progressed from tests on highly simplified model problems to demonstrating that the approach can compete successfully against the best existing numerical methods on 'full-scale' applications, as these arise for examples in the geosciences [4, 5, 6, 7]. A brief review of this development is therefore timely.

There are several ways to introduce RBFs. One way is to note that they generalize cubic splines in many ways, such as to scattered node layouts in any number of spatial dimensions and, in terms of accuracy, from fourth order to spectral (above any algebraic order). Since our present context concerns solving PDEs, we choose a different path here, starting instead from standard finite difference (FD) approximations. In their limit of increasing orders of accuracy, FD transform to pseudospectral (PS) methods, which alternatively can be described in terms of expansions in orthogonal functions - e.g. of Fourier- or Chebyshev- type. PS methods can be extremely effective, but are usually limited to simple domain shapes. With RBFs, we use data location dependent expansion functions, and give up all orthogonality features. In exchange, it transpires that one can gain a wide range of advantages, including complete geometric flexibility with regard to both domain shapes and node layouts, as well as freedom from mesh generation. The traditional PS methods can be recovered as special cases of RBFs. Computational cost and numerical stability were initially seen as potential difficulties, but major

progress has recently been made also in these areas.

2. FD and PS methods

FD approximations are typically derived in 1D by finding *weights* which make them exact for monomials of as high degrees as possible. In more than 1D, they can be applied in each direction in turn. In contrast, FD approximations that are directly designed to be exact for multivariate monomials have seldom been successful. It is often not clear which monomials to include and, for scattered nodes, the linear systems that determine the FD weights will often become singular.

2.1. FD formulas

Several numerical and symbolic algorithms are available for calculating FD weights on equispaced grids [8]. In case of a FD stencil of the general shape described by the numbers s (real), and d, n (non-negative integers):

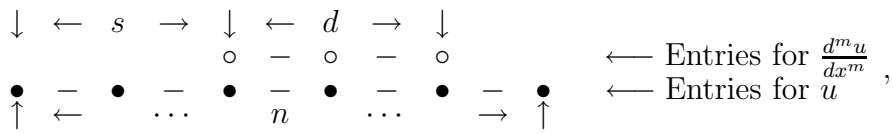

the briefest algorithm requires only two lines of code. In Mathematica 7:

$$t = \text{PadeApproximant}[x^s \left(\tfrac{\text{Log}[x]}{h}\right)^m, \{x, 1, \{n, d\}\}];$$
$$\text{CoefficientList}[\{\text{Denominator}[t], \text{Numerator}[t]\}, x]$$

This routine produces also the coefficients for all the main classes of linear multistep methods for ODEs. In our present context, these FD formulas are of particular interest due to the relation that is indicated in (1). The

'classical' centered FD formulas of increasing order for approximating $\frac{\partial u}{\partial x}$

$$
\begin{array}{lcccccccccc}
[1]\frac{\partial u}{\partial x} & = [& & & -\frac{1}{2} & 0 & \frac{1}{2} & & &]\frac{u}{h} + O(h^2) & \\
& = [& & \frac{1}{12} & -\frac{2}{3} & 0 & \frac{2}{3} & -\frac{1}{12} & &]\frac{u}{h} + O(h^4) & \\
& = [& -\frac{1}{60} & \frac{3}{20} & -\frac{3}{4} & 0 & \frac{3}{4} & -\frac{3}{20} & \frac{1}{60} &]\frac{u}{h} + O(h^6) & . \qquad (1) \\
& & \downarrow & \downarrow & \downarrow & \downarrow & \downarrow & \downarrow & \downarrow & & \\
& [\cdots & -\frac{1}{3} & \frac{1}{2} & -\frac{1}{1} & 0 & \frac{1}{1} & -\frac{1}{2} & \frac{1}{3} & \cdots]\frac{u}{h} & \text{PS limit}
\end{array}
$$

converge to a simple limit when the order is increased. A main theme of [9] was to generalize and expand on this observation.

At or near boundaries, one needs to use non-centered FD formulas. The weights will then instead diverge for increasing orders, as a consequence of the *Runge phenomenon*. A commonly used remedy is to cluster nodes near the boundary, e.g. as Chebyshev nodes $x_k = -\cos\frac{k\pi}{n},\ k = 0, 1, \ldots, n$ on [-1,1]. Effective algorithms for finding optimal FD weights are available also for such non-uniform grid cases [8], [10].

2.2. PS methods

We consider here only Fourier-PS and Chebyshev-PS methods.

2.2.1. Fourier-PS methods

For 2π-periodic data f_k given at $x_k = \frac{2(k-1)\pi}{n}$, $k = 1, 2, \ldots, n$, two ways to approximate $\frac{df}{dx}$ are:

i. Bring f_k to Fourier space by an FFT, differentiate analytically, and return the derivative values to physical space by an inverse FFT, or

ii. Apply the 'PS limit' stencil (last line of (1)) to the data (including its periodic extensions).

These two approaches will always give identical results (any order derivative, regular or staggered grids, etc.) Hence, it is natural to view the Fourier-

PS method as the limit of centered FD approximations as their order increases. The approach (i) is the most practical one. If we for simplicity assume n to be odd, we can view $1, \{\cos(kx), \sin(kx)\}, k = 1, 2, \ldots, \frac{n-1}{2}$ as the Fourier-PS method's *basis functions*.

2.2.2. Chebyshev-PS methods

With the nodes placed at Chebyshev locations, we have again two main options for approximating derivatives:

i. With a FCT (fast cosine transform - a variation of the FFT), obtain the interpolating polynomial in the form of its Chebyshev expansion coefficients, modify these according to analytic differentiation and return to physical space by another FCT.

ii. Create the differentiation matrix (DM) such that multiplying it with a column of function values at the nodes will return the matching derivative values. Each row in this DM contains the *weights* of a corresponding global FD stencil.

Also the Chebyshev-PS method can therefore be viewed either in terms of an expansion in basis functions (now $T_k(x),\ k = 0, 1, \ldots, n$), or as the application of high order FD stencils. Both versions are numerically practical, with operation counts of $O(n \log n)$ and $O(n^2)$, respectively. The latter option is usually the faster one when $n \lessapprox 200$.

2.2.3. PS methods in more than 1D

Grid layouts for PS methods in 2D are essentially limited to mappings of rectangular grids, giving very limited opportunities for handling irregular geometries and for carrying out local node refinements. Scattered nodes can

in general not be used [11]. Suppose they are located at $\underline{x}_k$ and that the basis function set is $F_k(\underline{x}),\ k = 1, 2, \ldots, n$. The coefficients λ_k for the interpolant $s(\underline{x}) = \sum_{k=1}^{n} \lambda_k F_k(\underline{x})$ are obtained by solving the linear system

$$\begin{bmatrix} F_1(\underline{x}_1) & F_2(\underline{x}_1) & \cdots & F_n(\underline{x}_1) \\ F_1(\underline{x}_2) & F_2(\underline{x}_2) & \cdots & F_n(\underline{x}_2) \\ \vdots & & \ddots & \vdots \\ F_1(\underline{x}_n) & F_1(\underline{x}_n) & \cdots & F_n(\underline{x}_n) \end{bmatrix} \begin{bmatrix} \lambda_1 \\ \lambda_2 \\ \vdots \\ \lambda_n \end{bmatrix} = \begin{bmatrix} f_1 \\ f_2 \\ \vdots \\ f_n \end{bmatrix}. \tag{2}$$

In more than 1D, it is possible to move the nodes continuously so that two nodes end up interchanged, without them having coincided at any time. The effect on the coefficient matrix above is that two rows become interchanged, i.e. its determinant has changed sign. It must therefore have been zero somewhere along the way. One can attempt to partly bypass this limitation by means of domain decomposition, e.g. *spectral elements*, but other complications will then arise (such as the need to introduce internal unphysical boundaries).

3. Introduction to RBF interpolation

RBF interpolation is based on a linear combination of translates of a single radially symmetric function, $\phi(||\underline{x} - \underline{x}_k||_2)$, that collocates the data $\{f_k\}_{k=1}^{n}$ at the nodes $\{\underline{x}_k\}_{k=1}^{n}$, $\underline{x}_k \in \mathbb{R}^n$, as shown in Figure 1 and given by (where we have dropped the subscript 2 on ℓ_2 norm)

$$s(\underline{x}) = \sum_{k=1}^{n} \lambda_k \phi(||\underline{x} - \underline{x}_k||). \tag{3}$$

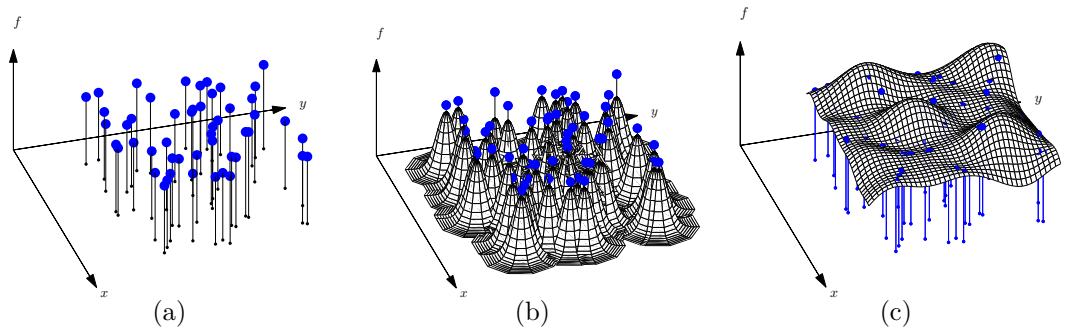

Figure 1: (a) Data values $\{f_k\}_{k=1}^n$ and locations $\{\underline{x}_k\}_{k=1}^n$ (b) RBF collocation functions (c) Unique linear combination of the RBFs, agreeing with all provided data.

The expansion coefficients, λ_k, can be found by inverting the matrix, A, in (4)

$$\begin{bmatrix} \phi(||\underline{x}_1 - \underline{x}_1||) & \phi(||\underline{x}_1 - \underline{x}_2||) & \cdots & \phi(||\underline{x}_1 - \underline{x}_n||) \\ \phi(||\underline{x}_2 - \underline{x}_1||) & \phi(||\underline{x}_2 - \underline{x}_2||) & \cdots & \phi(||\underline{x}_2 - \underline{x}_n||) \\ \vdots & \vdots & & \vdots \\ \phi(||\underline{x}_n - \underline{x}_1||) & \phi(||\underline{x}_n - \underline{x}_2||) & \cdots & \phi(||\underline{x}_n - \underline{x}_n||) \end{bmatrix} \begin{bmatrix} \lambda_1 \\ \lambda_2 \\ \vdots \\ \lambda_n \end{bmatrix} = \begin{bmatrix} f_1 \\ f_2 \\ \vdots \\ f_n \end{bmatrix}. \tag{4}$$

Since RBFs only depend on a scalar distance (defined by the ℓ_2 norm), discretization is independent of *coordinate system*, *dimension* and *domain geometry*. As an example, even if node locations on a sphere are given in spherical coordinates, no such grids need to be used. Distances are measured straight through the sphere and not along great arcs. As a result, RBFs are very simple to program.

For all the choices of RBFs listed in Table 1 (with a minor modification needed in (3) in case of GDS), the matrix in (4) can never be singular, no matter how any number of (distinct) nodes are scattered in any number of dimensions [12, 13, 14]. The 'piecewise smooth' radial functions feature a singularity at the origin and in the compactly supported 'Wendland' case

[15] also at $r = 1$. Radial functions listed under 'piecewise smooth' are of significant interest in the contexts of interpolation and statistics, but less so when solving PDEs (the fact that they are not C^∞ yields algebraic as opposed to spectral accuracy [15, 16]), and will not be discussed further. Infinitely smooth RBFs depend on a shape parameter ε that plays an important role in accuracy and conditioning of the matrix A in (4).

All numerical schemes for interpolation and for solving PDEs exhibit two main types of errors, *truncation* and *rounding* errors. The first is caused by a continuous problem having being replaced by a discrete one and the latter by finite floating point precision. We will later see that the flat RBF limit (small ε) can offer small truncation errors although numerical ill-conditioning can then amplify rounding errors, often to the extent of destroying all precision. The two main remedies against this are: 1) Instead of directly inverting the interpolation matrix (known as RBF-Direct), employ a stable algorithm (as discussed in Section 4.2); and 2) gradually increase ε when the number of nodes n is increased, in order to keep the numerical conditioning intact. This latter approach is commonly used and often works quite well, but the saturation error effect [3] may then prevent the overall error from converging to zero.

4. Flat RBFs ($\varepsilon \to 0$)

Classical basis functions are often designed to have various orthogonality properties, implying that functions of increasing orders become more oscillatory. Figure 2 (a) illustrates this for Legendre and Chebyshev polynomials. This can be contrasted to the situation when RBFs are made flatter ($\varepsilon \to 0$),

Type of basis function	**Radial function $\phi(\mathbf{r} = \|\underline{\mathbf{x}} - \underline{\mathbf{x}}_\mathbf{k}\|_\mathbf{2})$**
Piecewise smooth RBFs	
Generalized Duchon spline (GDS)	$r^{2m} \log r,\ m \in N$
	$r^{2m},\ m > 0$ and $m \notin N$
Wendland	$(1-r)_+^m p(r)$, p certain polynomials, $m \in N$
Matern	$\frac{2^{1-m}}{\Gamma(m)} r^m K_m(r), m > 0$
Infinitely smooth RBFs	
Gaussian (GA)	$e^{-(\varepsilon r)^2}$
Multiquadric (MQ)	$\sqrt{1+(\varepsilon r)^2}$
Inverse Multiquadric (IMQ)	$1/\sqrt{1+(\varepsilon r)^2}$
Inverse Quadratic (IQ)	$1/(1+(\varepsilon r)^2)$

Table 1: Some common choices for radial functions

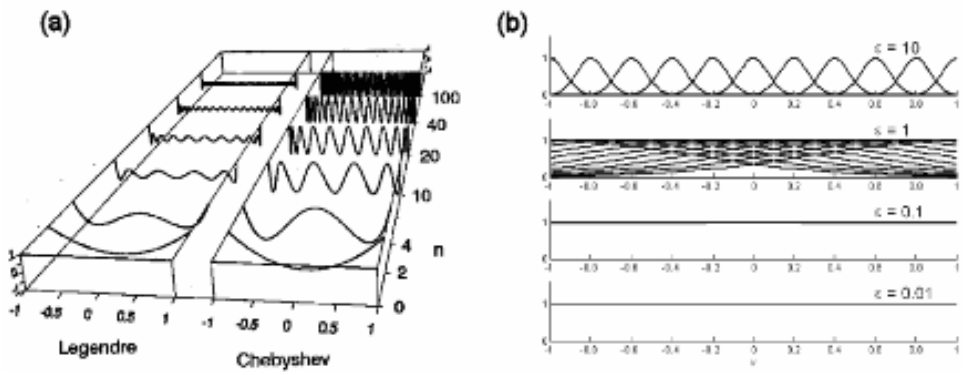

Figure 2: (a) Legendre and Chebyshev polynomials of increasing orders, (b) Eleven equi-spaced translates of GA RBFs for four different values of ε. From top to bottom, $\varepsilon = 10$, 1, 0.1 and 0.01.

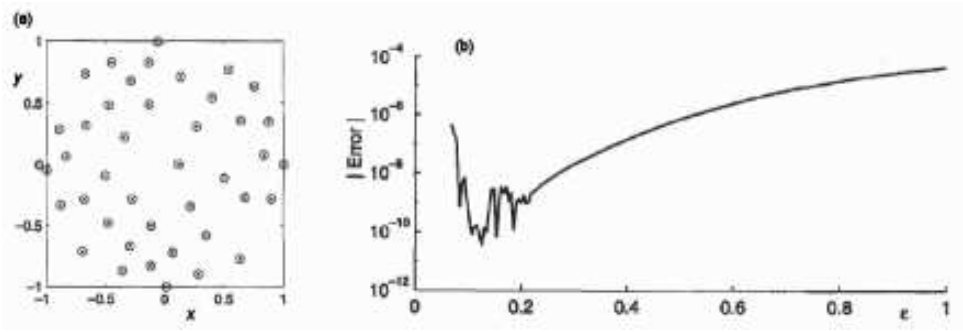

Figure 3: (a) A set of 41 scattered nodes in the unit circle, (b) The error in max norm when the test function $f(x,y) = 59/(67 + (x+\frac{1}{7})^2 + (y-\frac{1}{11})^2)$ is interpolated using these nodes, displayed as a function of the shape parameter ε.

as seen in Figure 2 (b) for GA RBFs in 1D. The conditioning of the coefficient matrix A in (4) worsens rapidly in this process. For example, in the case of $n = 41$ scattered nodes in 1D, with any of the 'Infinitely smooth RBFs' in Table 1, $\text{cond}(A) = O(\varepsilon^{-80})$ and $\det(A) = O(\varepsilon^{1640})$. In 2D, the corresponding rates become $O(\varepsilon^{-16})$ and $O(\varepsilon^{416})$, resp. Increasing n also worsens the conditioning. In 2D, $\text{cond}(A) = O(\varepsilon^{-2\,[(\sqrt{8n-7}-1)/2]})$, where $[\cdot]$ denotes the integer part [17]. As suggested by Figure 3, the low ε-range is nevertheless of great interest. Part (a) shows 41 scattered nodes over the unit circle in 2D and part (b) shows how the max norm error varies with ε when using RBF-Direct, i.e. interpolating a test function by directly applying (4) and (3) in standard 64 bit double precision. As ε is made smaller, accuracy increases to very high levels until numerical ill-conditioning kicks in. This observation naturally prompts a number of questions:

1. In exact arithmetic (with ill-conditioning not an issue), will RBF interpolants $s(\underline{x})$ converge some limit function as $\varepsilon \to 0$?

2. Is it possible to develop numerical algorithms that remain numerically well conditioned even as $\varepsilon \to 0$?
3. What error levels can be reached with RBF interpolation and derivative approximation?

4.1. PS - A special case of RBFs as $\varepsilon \to 0$

For scattered data in 1D, it was shown in [18] that the RBF interpolant will converge to Lagrange's interpolation polynomial as $\varepsilon \to 0$. The result is subject to some minor 'fine print' that has been strictly proven in the GA case [19, 20] but also holds for other infinitely smooth RBFs. Since the PS interpolant follows from the Lagrange intepolation polynomial (cf. Section 2), this result implies that RBF interpolants will reproduce PS interpolants in this limit. For example, periodically equispaced nodes will reproduce Fourier-PS methods. The convergence of RBF approximations to the Fourier-PS method in the 1D periodic case is analyzed in [21].

It was shown in [22] that, if the limit for $\varepsilon \to 0$ exists for a finite node configuration, the RBF interpolant must converge to a polynomial form also in multivariate cases. Numerical tests indicated that the limit indeed always exists when using GA RBFs (later proven in [23]) and also for a certain class of Bessel RBFs [24]. However, convergence may fail in connection with finite Cartesian lattices (and with other 'non-unisolvent' node configurations) for other RBF types. Other disadvantages with such finite lattices, in the context of RBFs, are noted in Section 5.

4.2. Stable numerical algorithms in the limit as $\varepsilon \to 0$

As $\varepsilon \to 0$, the RBF expansion coefficients λ_k will diverge rapidly towards $\pm\infty$ (as seen by the behavior of the condition number for the 1D and 2D

cases above). Hence, a vast amount of numerical cancellations must occur in the sum (3) for it not to diverge. The two numerically stable algorithms for calculating $s(\underline{x})$ in the $\varepsilon \to 0$ limit were motivated by the realization that RBF-Direct (solving for the coefficients in (4) followed by summing the terms in (3)) amounts to two successive numerically ill-conditioned steps for calculating a well conditioned quantity $s(\underline{x})$. Thus, there also ought to exist numerically well-conditioned algorithms for the task.

Varies types of preconditioning/SVD decomposition of (4), as well as the use of high precision arithmetic have been suggested in the literature. The basic problem with the first of these approaches is that essential information becomes irretrievably lost the moment the coefficient matrix A is formed, and no regularization ideas can recover this. Nor does this approach address that also (3) is ill conditioned. High precision arithmetic can offer some help if very fast high precision hardware is available, but the degradation of condition numbers with increasing n and decreasing ε is often too severe for this venue to be practical. Only two algorithmic concepts, summarized next, have so far been found that permit well conditioned calculations all the way into the $\varepsilon \to 0$ limit.

Contour-Padé algorithm. The key concept is to consider the RBF interpolant not only for real values of ε but also for complex ones. Then, $s(\underline{x})$ in (3) becomes a *meromorphic* function of ε in the vicinity of $\varepsilon = 0$, with this point itself usually being only a removable singularity. That observation led to the first successful stable algorithm [25]. Its main shortcoming is a limitation on the number of nodes n that the algorithm will work for; in 1D $n \lessapprox 20$ and in 2D $n \lessapprox 80$. These relatively low limits have still allowed much exploratory

work on RBFs in the low ε regime. The algorithm conclusively showed that there exists no inevitable 'uncertainty principle'-type conflict between high RBF approximation accuracy and numerical conditioning.

RBF-QR algorithm. Figure 4 shows that one must separate carefully between a *space* and a *basis* that spans it. In both of the displayed examples, the spaces are excellent, yet the basis chosen to span them can be good or bad. Turning to RBFs, the translates of near-flat RBFs clearly form a basis that is ill-suited for immediate numerical use. The key question is whether the underlying approximation *space* is bad, or if we can resolve all conditioning issues just by finding an alternate good basis in exactly the same space. This latter case turns out to hold true, leading to the follow-up issue of how one *analytically* can carry out the key steps of the basis conversion so that no numerical cancelations will arise in the process. The first RBF case for which this was done successfully was for scattered nodes over a sphere [26], based on certain expansion formulas that were originally devised for different purposes in [27, 28]. In this case, there is no limit on the number of nodes. A corresponding algorithm for regular general 1D,2D, and 3D domains is given in [29].

5. PS vs. RBF derivative approximations

It follows immediately from the observations above that PS methods can be seen as a very special case of RBF methods - just place the nodes in the manner required for some classic PS method, and then let $\varepsilon \to 0$. Typically, neither the flat basis function limit, nor grid-based node placing are optimal. Even on regular lattices, RBFs can provide (slightly) better derivative

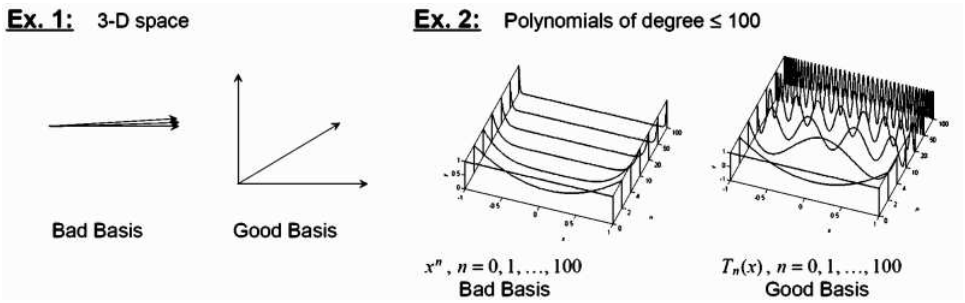

Figure 4: Examples of 'good' approximation *spaces* spanned by good vs. bad *basis*.

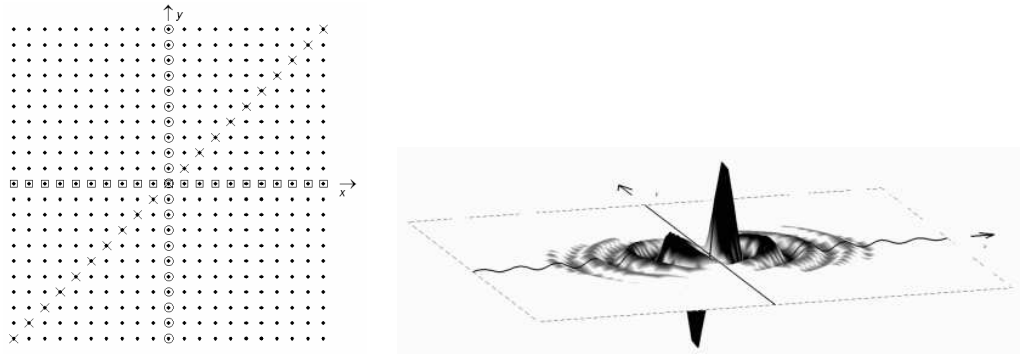

(a) (b)

Figure 5: (a) Nodes typically used for approximating $\frac{\partial}{\partial x}(\square)$ and $\frac{\partial}{\partial y}(\text{o})$ at the origin on a 2D Cartesian grid, with $\times$ marking the direction for the directional derivative $\frac{1}{\sqrt{2}}(\frac{\partial}{\partial x} + \frac{\partial}{\partial y})$ (b) Where data for approximating $\frac{\partial}{\partial x}$ should be picked up in a grid-free (x,y) plane.

approximations than PS methods. Consider for example the task of approximating $\frac{\partial}{\partial x}$ at the origin of a 2D Cartesian grid. Figure 5a illustrates by squares ("$\square$") which nodes will be used by FD and PS methods. In the case of $\frac{\partial}{\partial y}$, the nodes will instead be those marked with ("$\circ$"). The PS approximation for $L = \frac{1}{\sqrt{2}}(\frac{\partial}{\partial x} + \frac{\partial}{\partial y})$ will be a combination of these two approximations, There is something quite strange about this. The operator L represents the directional derivative in the direction with nodes marked ("$\times$"), yet not a single one of these nodes have been utilized Some nearby function values along this line ought contain more significant information than what is the case for function values far out along the x- and y-axes. Some very heuristic arguments in [30] suggest that the function $\frac{x}{8}\ {}_0F_1(3, -\frac{1}{4}(x^2+y^2))$, shown in Figure 5b, better reflects how information should be collected in the vicinity of the origin when approximating $\frac{\partial}{\partial x}$. Unless the RBF shape parameter ε is reduced all the way to the PS limit (or GA RBFs are used on a Cartesian lattice), RBF-based derivative approximations will typically pick up information in a way that is more reminiscent of Figure 5b than of the line marked by squares in Figure 5a (along the x-axis only). Although the accuracy advantage with RBFs is not very large in this particular case of doubly periodic Cartesian grids, it is still noteworthy that the RBF approach even here more than holds its own in comparison with periodic PS methods. Hexagonal and somewhat scattered node layouts, impossible with the PS approach, can improve RBF accuracy further still as well as provide better conditioning, c.f. Section 6.2.

6. Introductory examples of RBFs for PDEs

Kansa proposed in 1990 to use the analytic derivatives of an RBF interpolant to approximate the spatial derivatives of steady-state and convective-diffusive PDEs [1, 2]. For time-stepping, the DMs can be formed as a pre-processing step and then be applied fast as matrix times vector multiplications. For steady-state cases, the RBF expansion is enforced at each node such that both PDE and boundary conditions are satisfied. This approach has been widely successful, even if rare possibilities for singularities were later noted [31]. Although a 'symmetric' version [32], [33] can never be singular, its practical advantage is unclear. Like for interpolation, infinitely smooth radial functions typically provide spectral accuracy [16, 34, 35].

6.1. First uses of stable algorithms

The study [36] introduced the novelty of applying a stable algorithm to the task of solving PDEs by RBFs. Figure 6 shows a typical result. Kansa's direct approach is used here for a Poisson equation in 2D:

$$\Delta u(\underline{x}) = f(\underline{x}) \qquad \text{in interior } \Omega \tag{5}$$

$$u(\underline{x}) = g(\underline{x}) \qquad \text{on boundary } \partial\Omega. \tag{6}$$

A simple test case is obtained by choosing $u(\underline{x}) = 100/(100+(x-0.2)^2+2y^2)$ and then selecting $g(\underline{x})$ and $f(\underline{x})$ accordingly. The domain is the unit circle (in order to allow easy comparisons of RBFs against FD2 and PS methods, which require simple domain shapes). We use here in all three cases node sets with $N_B = 16$ nodes on $\partial\Omega$ and $N_I = 48$ nodes in Ω with distributions: (RBF) generally scattered, (PS) equispaced in angle, Chebyshev across the

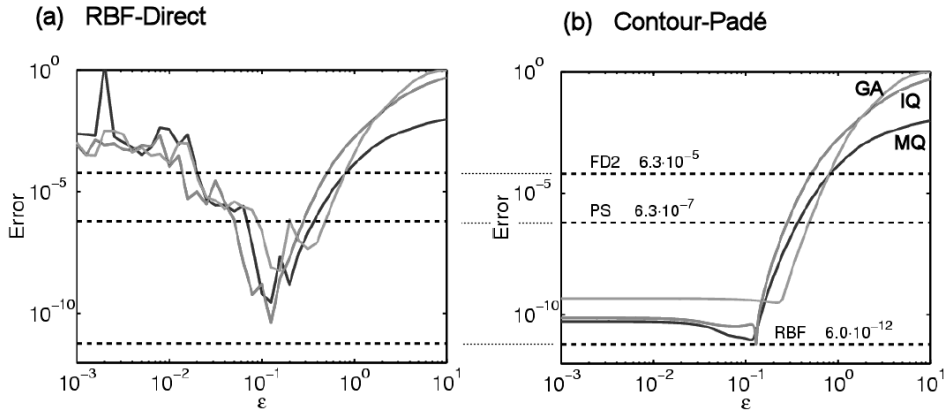

Figure 6: ℓ_∞ errors as a function of ε, when solving (6) using GA, IQ, MQ RBFs (a) Using RBF-Direct and (b) Using Contour-Padé. The dashed lines across both subplots compares the accuracies reached by FD2 and PS (both independent of ε).

circle; and (FD2) equispaced in both angle and across circle. The use of a stable algorithm not only improves the accuracy, but also makes the choice of 'optimal' ε very much less critical. The first use of the RBF-QR algorithm for solving PDEs is noted Section 7.1.1.

6.2. Boundary issues and node distributions

Interpolation is always much more stable than extrapolation. Likewise, errors at a domain boundary tend to be larger than in domain interiors. In the case of high degree polynomial interpolation, this edge effect gives rise to the Runge phenomenon, often controlled by Chebyshev-type node clustering. With RBFs, especially when they are used to solve PDEs, there are additional (and usually better) options available to control these edge effects [37, 38]. While some aspects of RBF theory have benefitted from analysis on Cartesian lattices [39, 40, 41, 42], it should be noted again that

such lattices usually are unfavorable node distributions [18] (Ex. 7), [30, 43]. Hexagonal lattices can be significantly better, as can Halton node sets and node sets achieved by *greedy algorithms* [44]. Infinite lattice analysis is often misleading, for example in showing low order algebraic convergence rates even when finite node distributions feature spectral convergence.

7. RBFs applied to PDEs arising in the geosciences

The largest-scale implementations of RBF spatial discretization for solving PDEs have been pursued in the geosciences. These implementations are in 2D and 3D spherical geometries, using 1000s to over half million degrees of freedom in space. Performance comparisons are presented against the most advanced currently existing numerical methods. The results below are only partial summarizations of [4, 5, 6, 7], with these articles giving studies in convergence, time stability, and the choice of the shape parameter ε. In all cases presented, no filtering was needed to stabilize the RBF method.

7.1. Transport on a sphere

Since advection is a primary process in most astro/geophysical fluid applications, it is important to the accuracy of the advective solver that the solution is kept intact without artificial dispersion or dissipation. As a result, the first benchmarks to be addressed are two cases in pure transport on the sphere: 1) linear translation (solid-body rotation) [4] and 2) cyclogenic deformation (translating vortex roll-up) [4, 6]. Although the PDEs are posed in spherical coordinates, no pole singularities exist when using the RBF method since the basis functions are not defined in terms of any surface-based coordi-

nate system. In this section, we consider only scalar-valued variables. In case of vector valued dependent variables, see the discussions in [5, 45, 46, 47].

7.1.1. Solid body rotation

This standard benchmark describes the advection, by a non-divergent wind, of a solid body (i.e. the initial condition) around the sphere at an angle α relative to the polar axis [4, 48, 49, 50, 51]. The governing PDE in latitude (θ) and longitude (λ) is

$$\frac{\partial h}{\partial t} + (\cos\alpha - \tan\theta \sin\varphi \sin\alpha)\frac{\partial h}{\partial \varphi} - \cos\varphi \sin\alpha \frac{\partial u}{\partial \theta} = 0, \tag{7}$$

where h is the initial condition, a rotated cosine function connecting to a flat plane at its base, implying a jump in the second derivative there. This irregularity makes it more typical of actual (non-smooth) data, and does not give any unfair advantages to high order methods. Figure 7 [4] shows the

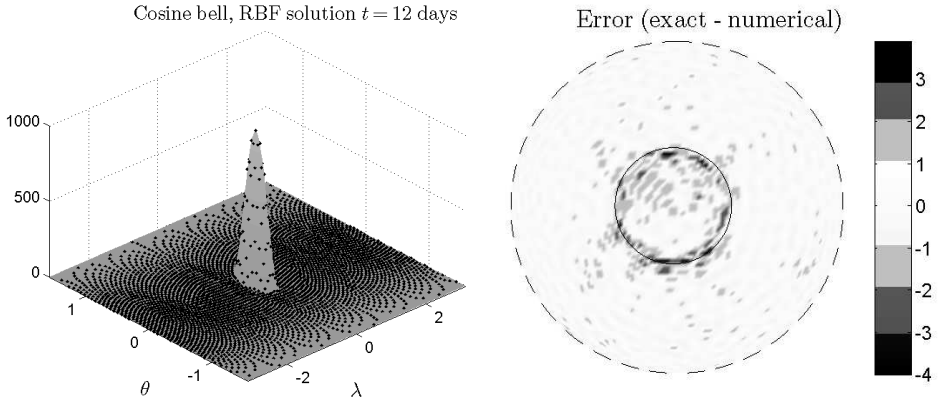

Figure 7: Left: Cosine bell (peak height 1000) displaced after one revolution in a 4096 node RBF calculation, Right: The error, with a maximum of 0.3%, is seen to be dominated by errors at its base caused by the jump there in the second derivative.

	Method	Relative l_2 error	Nr of nodes/ free parameters	Time step	Code length	Ref.
RBF	Rad. basis fn.	0.006	4,096	1/2 hour	$<$ 40	[4]
SPH	Spherical harm.	0.005	32,768	90 sec.	$>$ 500	[52]
DF	Double Fourier	0.005	32,768	90 sec.	$>$ 100	[52]
SE	Spectral elem.	0.005	7,776	6 min.	$>$ 1,000	[53]

Table 2: Comparison between one revolution cosine bell calculations in the literature

result of a typical calculation corresponding to one full revolution around the sphere, with the time scaled so that one revolution corresponds physically to 12 days. The same test case was run in [50] to thousands of revolutions, in which case the best ε-value necessitated the use of the RBF-QR method. The error picture remained essentially unchanged from the one shown in Figure 7b for just one revolution. Table 2 compares different numerical methods from the literature on this test case for achieving the a relative l_2 error of approximately 0.0005 after one revolution. The RBF calculation requires the least number of nodes, while using the longest time steps. It should be noted that the RBF time step in Table 2 was not limited by stability as in the case of the other methods but so that time discretization errors matched spatial discretization errors. In terms of stability, the RBF method could take a $3\frac{1}{2}$ hour time step with only about an order of magnitude loss in error (see Section 5.3 [4]).

7.1.2. Translating vortex roll-up

Here, two opposing vortices form as they are translated along the equator of a coordinate system rotated an arbitrary angle relative to the polar axis

(see [6, 54]). Since the angular velocity depends on the vortex centers, the rotating flow field is time-dependent. The initial condition varies as a steep tanh profile between the poles. The purpose of the test is to see how well a numerical method handles a solution with increasingly stronger gradients over time, as seen in Figures 8(a-d) for 1 revolution (12 days). The test was conducted with and without local node refinement. Table 3 compares

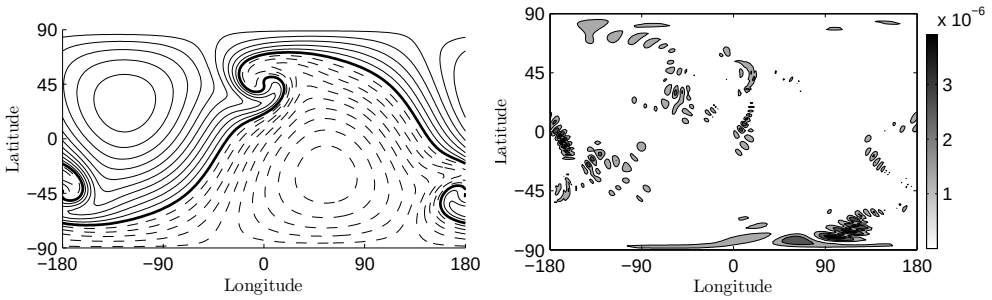

(a) $t = 3$ days (b) $t = 3$ days

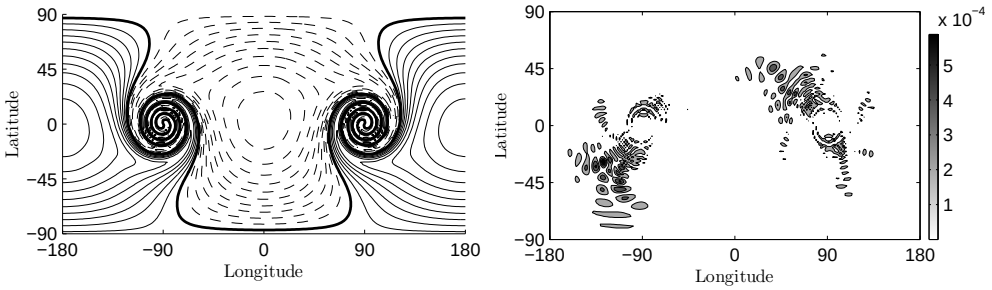

(c) $t = 12$ days (d) $t = 12$ days

Figure 8: RBF solution and magnitude of the error at $t = 3$ and 12 days for the moving vortex case with $N = 3136$ refined nodes and $\Delta t = 18$ minutes. For the plots of the solution, contours with an interval of 0.05 are shown and the dashed lines correspond to $h < 1$.

the latest as well as all implementations for this case, where FV is finite volume and DG is a hybrid spectral element discontinuous Galerkin method.

Method	Number of nodes	Angular Resolution	Time-step in min	Relative ℓ_2 error in h	Ref.
Without local refinement					
RBF	3,136	6.4^o	60	$4 \cdot 10^{-3}$	[6]
FV (lat-long grid)	165,888	0.625^o	10	$2 \cdot 10^{-3}$	[54]
FV (cubed sphere)	38,400	1.125^o	30	$2 \cdot 10^{-3}$	[55]
DG	9,600	2.6^o	6	$7 \cdot 10^{-3}$	[54]
With local refinement					
RBF	3,136	-	20	$8 \cdot 10^{-5}$	[6]
FV (lat-long)	-	$5^o - 0.625^o$	1-3	$2 \cdot 10^{-3}$	[54]

Table 3: Comparison between methods in the literature for translating vortex roll-up at t=12 days.

Without local refinement, for the same accuracy, RBFs use less nodes with larger time-steps. With local refinement, the RBF calculation gave much higher accuracy than any other previous implementation.

7.2. Shallow water equations (SWE) - Forced translating low pressure system

This common benchmark models a short wave trough that is embedded in a westerly jet [48]. Forcing terms are added to the SWE, a set of 3 nonlinear coupled PDEs, so that the initial condition is nonlinearly advected intact. An analytic solution is available (see Section 6b [5]). The results below refer to the RBF calculations in [5]. The initial velocity and height(pressure) field with the error after 5 days ($\sim 1/4$ of the way around the sphere) is given in Figure 9. An important aspect in geo-modeling is the conservation of total energy and mass. Table 4 gives the relative difference (final/initial-1) in the

total energy and mass of the system after 5 and 25 days. Unlike FV methods, the RBF method used here is not constructed to inherently conserve these quantities, yet for $N = 4096$, both quantities are conserved to 9 decimal places. Table 5 compares the RBF method to the most recent high-order method results for this test case in the literature. The RBF calculation easily offers the highest accuracy with the longest time step that has yet been presented. Actual wall clock times are harder to compare, since each study use very different hardware - in many cases super-computers. The RBF calculations reported here were run in Matlab on a standard 2.66 GHz PC, with the $N = 3136$ run taking 2 minutes and the $N = 5041$ run taking 12 minutes. These times include pre-processing steps.

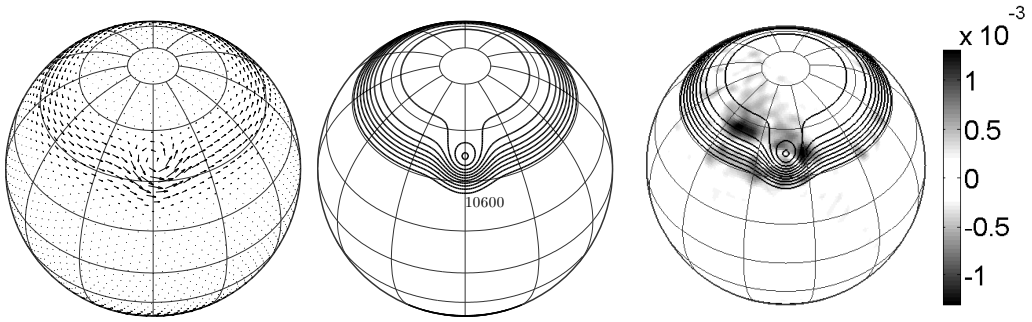

(a) (b) (c)

Figure 9: (a) The initial velocity field; (b) The initial height(pressure) field, contours at 50m intervals; (c) The error in (b) after 5 days for $N = 3136$.

7.3. Mantle convection in 3D spherical geometry

The physical scenario is the following: the flow is incompressible; temperature (T) is governed by a mixed convective-diffusive PDE; the momentum

Nr. of Nodes	Mass	5 days	25 days	Energy	5 days	25 days
$N = 3136$		$2 \cdot 10^{-9}$	$4 \cdot 10^{-9}$		$-3 \cdot 10^{-9}$	$2 \cdot 10^{-9}$
$N = 4096$		$1 \cdot 10^{-11}$	$2 \cdot 10^{-10}$		$-1 \cdot 10^{-10}$	$5 \cdot 10^{-10}$

Table 4: Relative Difference (final/initial-1) in total mass and energy after 5 and 25 days.

	Method	Nr. of Nodes	Time step	ℓ_2 Error	Ref.
RBF	Radial basis fn.	784	40 min	$4.8 \cdot 10^{-1}$	[5]
		3,136	15 min	$8.8 \cdot 10^{-6}$	
		5,041	6 min	$1.0 \cdot 10^{-8}$	
DF	Double Fourier	2,048	6 min	$3.9 \cdot 10^{-1}$	[52]
		8,192	3 min	$8.2 \cdot 10^{-4}$	
		32,768	90 sec	$4.0 \cdot 10^{-4}$	
SPH	Spherical harmonics	8,192	3 min	$2.0 \cdot 10^{-3}$	[56]
SE	Spectral elements	6,144	90 sec	$6.5 \cdot 10^{-3}$	[57]
		24,576	45 sec	$4.0 \cdot 10^{-5}$	

Table 5: Comparison between t = 5 day calculations for the SWE (in the SPH case, discretizations are needed in both lat-long grids and SPH coefficient space, using 8,192 and 1,849 parameters, respectively).

PDEs are modeled by Stokes flow, requiring an elliptic solver; the impermeable boundaries are slip with $T = 1$ at the core and $T = 0$ at the crust. The PDEs are approximated in [7] by RBF discretization on each of many concentric spherical shells, combined with Chebyshev PS discretization radially (see Figure 10). Since no analytic solutions are available, isoviscous flow at low $Ra = 7,000$ is used as a benchmark since it is a steady-state regime, requiring low resolution. The initial condition for this benchmark is a combination of fourth-order spherical harmonics times linear decay in the radial direction (see [7]). The results are summarized in Table 6, comparing the global variables, Nu_{crust}, Nu_{core}, $< V_{RMS} >$, $< T >$ (Nu is the Nusselt Number, V_{RMS} is the root mean square velocity, and $< >$ indicates globally averaged). For the scheme to conserve energy, Nu_{crust} should equal Nu_{core} for this test. We note that the RBF-CH method achieves near perfection in terms of accuracy while using a much lower level of discretization when compared to the Romberg extrapolated results of the SPH-FD method, the only other semi-spectral method. It was also the only implementation that was run on standard PC hardware.

Figure 10(c) shows $Ra = 10^6$, a more physically realistic situation when unstable convection dominates, as the current Earth is $Ra = 10^7$. This simulation is completely unique in that it is the only spectral model in the literature to be run at such a high Ra in spherical geometry. In addition, the RBF-CH calculation showed an instability at $Ra = 70,000$ that had been theorized by [62] but remained somewhat controversial, as it had not been seen in any numerical simulations until now. This episode may be the first case in which RBF solutions of PDEs provided new physical insights. It also

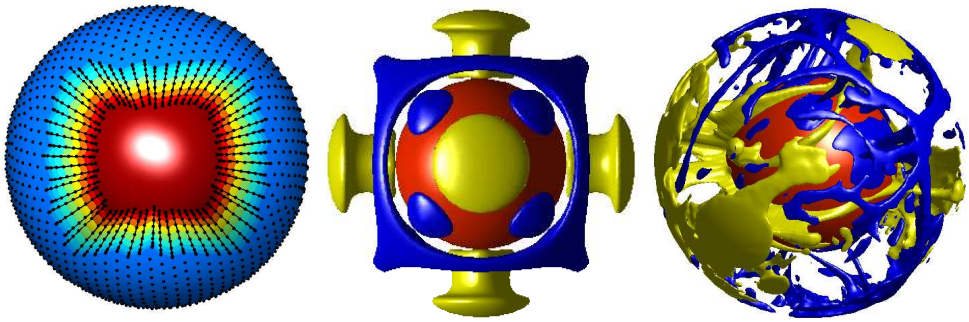

(a) (b) (c)

Figure 10: Mantle convection: (a) RBF-CH discretization (b) Solution at $Ra = 7000$, yellow=upwelling, blue=downwelling, red=core (c) Solution at $Ra = 10^6$, ≈4.5 times the age of Earth.

demonstrated quite strikingly how effective RBFs can be on standard PCs.

7.4. Future developments

While RBFs have been applied to highly simplified PDE model problems for decades, large-scale applications are now increasingly being pursued. Issues of particular interest for future work include improved reliability, effectiveness, and scalability of RBF implementations, dynamically adaptive node refinement [63], RBF-generated FD (RBF-FD) methods [64, 65, 66], RBF in conjunction with domain decomposition [67, 68, 69, 70], their application on GPUs, stability analysis in the presence of boundaries, effective 'fast' algorithms, additionally stable algorithms, etc.

8. Acknowledgements

NCAR is supported by the National Science Foundation (NSF). The work of Natasha Flyer was supported by NSF grants ATM-0620100 and DMS-

Method	Nr of nodes	Nu_{crust}	Nu_{core}	$< V_{RMS} >$	$< T >$	Ref.
RBF-CH	36,800	3.6096	3.6096	31.0820	0.21578	[7]
SPH-FD	extrapolated	3.6096	3.6096	31.0821	0.21577	[58]
SPH-FD	552,960	3.6086	-	31.0765	0.21582	[58]
FE	393,216	3.6254	3.6016	31.09	0.2176	[59]
FV	663,552	3.5983	3.5984	31.0226	0.21594	[60]
FD	12,582,912	3.6083	-	31.0741	0.21639	[61]

Table 6: Comparison between methods in the literature for the standard Ra=7000 case.

0934317. Bengt Fornberg was supported by the NSF Grants DMS-0611681, DMS-0914647 and ATM-0620068.

References

[1] E. J. Kansa, Multiquadrics – a scattered data approximation scheme with applications to computational fluid-dynamics – i: Surface approximations and parital derivative estimates, Comput. Math. Appl. 19 (1990) 127–145.

[2] E. J. Kansa, Multiquadrics – a scattered data approximation scheme with applications to computational fluid-dynamics – ii: Solutions to parabolic, hyperbolic and elliptic partial differential equations, Comput. Math. Appl. 19 (1990) 147–161.

[3] G. E. Fasshauer, Meshless Approximation Methods with MATLAB, Interdisciplinary Mathematical Sciences - Vol. 6, World Scientific Publishers, Singapore, 2007.

[4] N. Flyer, G. B. Wright, Transport schemes on a sphere using radial basis functions, J. Comp. Phys. 226 (2007) 1059–1084.

[5] N. Flyer, G. B. Wright, A radial basis function method for the shallow water equations on a sphere, Proc. Roy. Soc. A 465 (2009) 1949–1976.

[6] N. Flyer, E. Lehto, Rotational transport on a sphere: Local node refinement with radial basis functions, J. Comp. Phys. 229 (2010) 1954–1969.

[7] G. B. Wright, N. Flyer, D. A. Yuen, A hybrid radial basis function - pseudospectral method for thermal convection in a 3d spherical shell, Geophysics, Geochemistry, Geosystems under revision (2010).

[8] B. Fornberg, Calculation of weights in finite difference formulas, SIAM Rev. 40(3) (1998) 685–691.

[9] B. Fornberg, A Practical Guide to Pseudospectral Methods, Cambridge University Press, Cambridge, 1996.

[10] J. A. C. Weideman, S. C. Reddy, A matlab differentiation matrix suite, ACM TOMS 26 (2000) 465–519.

[11] J. Y. McLeod, M. L. Baart, Geometry and Interpolation of Curves and Surfaces, Cambridge University Press, 1998.

[12] S. Bochner, Monotone fuctionen, Stieltjes integrale und harmonische analyse, Math. Ann. 108 (1933) 378–410.

[13] C. A. Micchelli, Interpolation of scattered data: distance matrices and conditionally positive definite functions, Constr. Approx. 2 (1986) 11–22.

[14] I. J. Schoenberg, Metric spaces and completely monotone functions, Ann. Math. 39 (1938) 811–841.

[15] H. Wendland, Scattered Data Approximation, Cambridge University Press, Cambridge, 2005.

[16] J. Yoon, Spectral approximation orders of radial basis function interpolation on the Sobolev space, SIAM J. Math. Anal. 23 (2001) 946–958.

[17] B. Fornberg, J. Zuev, The Runge phenomenon and spatially variable shape parameters in RBF interpolation, Comput. Math. Appl. 54 (2007) 379–398.

[18] T. A. Driscoll, B. Fornberg, Interpolation in the limit of increasingly flat radial basis functions, Comput. Math. Appl. 43 (2002) 413–422.

[19] M. Buhmann, S. Dinew, Limits of radial basis function interpolants, Comm. Pure Appl. Analy. 6 (2007) 569–585.

[20] T. Hrycak, personal communication, 2004.

[21] B. Fornberg, N. Flyer, Accuracy of radial basis function interpolation and derivative approximations on 1-D infinite grids, Adv. Comput. Math. 23 (2005) 5–20.

[22] B. Fornberg, G. Wright, E. Larsson, Some observations regarding interpolants in the limit of flat radial basis functions, Comput. Math. Appl. 47 (2004) 37–55.

[23] R. Schaback, Multivariate interpolation by polynomials and radial basis functions, Constr. Approx. 21 (2005) 293–317.

[24] B. Fornberg, E. Larsson, G. Wright, A new class of oscillatory radial basis functions, Comput. Math. Appl. 51 (2006) 1209–1222.

[25] B. Fornberg, G. Wright, Stable computation of multiquadric interpolants for all values of the shape parameter, Comput. Math. Appl. 48 (2004) 853–867.

[26] B. Fornberg, C. Piret, A stable algorithm for flat radial basis functions on a sphere, SIAM J. Sci. Comput. 200 (2007) 178–192.

[27] W. Freeden, T. Gervens, M. Schreiner, Constructive Approximation on the Sphere with Applications to Geomathematics, Oxford University Press, 1998.

[28] S. Hubbert, B. Baxter, Radial basis functions for the sphere, in: W. Haussmann, K. Jetter, M. Reimer (Eds.), Recent Progress in Multivariate Approximation, Proc. of the 4th Intl. Conf., volume 137 of *Intl. Series of Num. Math.*, Birkhäuser, Witten-Bommerholz, Germany, 2001, pp. 33–47.

[29] B. Fornberg, E. Larsson, N. Flyer, Stable computations with Gaussian radial basis functions, SIAM J Sci. Comp. under revision (2010).

[30] B. Fornberg, N. Flyer, J. M. Russell, Comparisons between pseudospectral and radial basis function derivative approximations, IMA J. Num. Anal. 30(1) (2010) 149–172.

[31] Y. C. Hon, R. Schaback, On unsymmetric collocation by radial basis functions, Appl. Math. Comput. 119 (2001) 177–186.

[32] G. E. Fasshauer, Solving partial differential equations by collocation with radial basis functions, in: A. LeMéhauté, C. Rabut, L. L. Schumaker (Eds.), Surface fitting and multiresolution method, Proc. 3rd Intl. Conf. on Curves and Surfaces, volume 2, Vanderbilt University Press, Nashville, TN, Chamonix–Mont-Blac, 1997.

[33] Z. Wu, Hermite-birkoff interpolation of scattered data by radial basis functions, Approx. Theory Appl. 8 (1992) 1–10.

[34] M. D. Buhmann, N. Dyn, Spectral convergence of multiquadric interpolation, Proc. Edinburgh Math. Soc. 36 (1993) 319–333.

[35] W. R. Madych, S. A. Nelson, Multivariate interpolation and conditionally positive functions ii, Math. Comp. 54 (1990) 211–230.

[36] E. Larsson, B. Fornberg, A numerical study of some radial basis function based solution methods for elliptic PDEs, Comput. Math. Appl. 46 (2003) 891–902.

[37] A. I. Fedoseyev, M. J. Friedman, E. J. Kansa, Improved multiquadric method for elliptic partial differential equations via pde collocation on the boundary, Comp. Math. Appli. 43 (2002) 439–455.

[38] B. Fornberg, T. A. Driscoll, G. Wright, R. Charles, Observations on the behavior of radial basis functions near boundaries, Comput. Math. Appl. 43 (2002) 473–490.

[39] B. J. C. Baxter, On the asymptotic cardinal function of the multiquadric $\varphi(r) = (r^2 + c^2)^{1/2}$ as $c \to \infty$, Comp. Math. Appl. 24(12) (1992) 1–6.

[40] M. D. Buhmann, M. J. D. Powell, Radial basis function interpolation on an infinite regular grid, in: J. Mason, M. Cox (Eds.), Algorithms for Approximation II, Chapman and Hall, London, 1990, pp. 47–61.

[41] B. Fornberg, N. Flyer, S. Hovde, C. Piret, Locality properties of radial basis function expansion coefficients for equispaced interpolation, IMA J. Num. Anal 28 (2008) 121–142.

[42] N. Flyer, Exact polynomial reproduction for oscillatory radial basis functions on infinite lattices, Comp. Math. Appl. 51 (2006) 1199–1208.

[43] A. Iske, Multiresolution Methods in Scattered Data Modeling, Springer Verlag, Berlin, 2004.

[44] R. Schaback, H. Wendland, Adaptive greedy techniques for approximate solution of large RBF systems, Numer. Algor. 24 (2000) 239–254.

[45] F. J. Narcowich, J. D. Ward, G. B. Wright, Divergence-free rbfs on surfaces, J. Fourier Anal. Appl 13 (2007) 643–663.

[46] E. J. Fuselier, G. B. Wright, Stability and error estimates for vector field interpolation and decomposition on the sphere with RBFs, SIAM J. Numer. Anal. 47 (2009) 3213–3239.

[47] E. J. Fuselier, F. J. Narcowich, J. D. Ward, G. B. Wright, Error and stability estimates for surface-divergence free rbf interpolants on the sphere, Math. Comp. 78 (2009) 2157–2186.

[48] D. L. Williamson, J. B. Drake, J. J. Hack, R. Jakob, P. N. Swarztrauber,

A standard test set for numerical approximations to the shallow water equations in spherical geometry, J. Comp. Phys. 102 (1992) 211–224.

[49] B. Fornberg, D. Merrill, Comparison of finite difference- and pseudospectral methods for convective flow over a sphere, Geophy. Res. Lett. 24 (1997) 3245–3248.

[50] B. Fornberg, C. Piret, On choosing a radial basis function and a shape parameter when solving a convective PDE on a sphere, J. Comp. Phys. 227 (2008) 2758–2780.

[51] A. St-Cyr, C. Jablonowski, J. M. Dennis, H. M. Tufo, S. J. Thomas, A comparison of two shallow-water models with nonconforming adaptive grids, Mon. Wea. Rev. 136 (2008) 1898–1922.

[52] W. F. Spotz, M. A. Taylor, P. N. Swarztrauber, Fast shallow water equation solvers in latitude-longitude coordinates, J. Comp. Phys. 145 (1998) 432–444.

[53] R. D. Nair, S. J. Thomas, R. D. Loft, A discontinuous Galerkin global shallow water model, Mon. Wea. Rev. 133 (2005) 876–888.

[54] R. D. Nair, C. Jablonowski, Moving vortices on the sphere: A test case for horizontal advection problems., Mon. Wea. Rev. 136 (2008) 699–711.

[55] W. M. Putman, S. J. Lin, Finite-volume transport on various cubed-sphere grids, J. Comp. Phys. 227 (2007) 55–78.

[56] R. Jakob-Chien, J. J. Hack, D. L. Williamson, Spectral transform solutions to the shallow water test set, J. Comp. Phys. 119 (1995) 164–187.

[57] M. Taylor, J. Tribbia, M. Iskandarani, The spectral element method for the shallow water equations on the sphere, J. Comp. Phys. 130 (1997) 92–108.

[58] H. Harder, U. Hansen, A finite-volume solution method for thermal convection and dynamo problems in spherical shells, Geophys. J. Int 161 (2005) 522–532.

[59] S. Zhong, A. McNamara, E. Tan, L. Moresi, M. Gurnis, A benchmark study on mantle convection in a 3-D spherical shell using CitcomS, Geochem. Geophys. Geosyst. 9 (2008) Q10017.

[60] K. Stemmer, H. Harder, U. Hansen, A new method to simulate convection with strongly temperature-dependent and pressure-dependent viscosity in spherical shell, Physics of the Earth and Planetary Inter. 157 (2006) 223–249.

[61] M. C. Kameyama, A. Kageyama, T. Sato, Multigrid-based simulation code for mantle convection in spherical shell using Yin-Yang grid, Phys. Earth Planet. Inter. 171 (2008) 19–32.

[62] D. Bercovici, G. Schubert, G. A. Glatzmaier, A. Zebib, Three-dimensional thermal-convection in a spherical shell, J. Fluid Mech. 206 (1989) 75–104.

[63] T. A. Driscoll, A. Heryundono, Adaptive residual subsampling methods for radial basis function interpolation and collocation problems, Comput. Math. Appl. 53 (2007) 927–939.

[64] Y. V. S. S. Sanyasiraju, G.Chandhini, Local radial basis function based gridfree scheme for unsteady incompressible viscous flows, J. Comp. Phys. 227(20) (2008) 8922–8948.

[65] C. Shu, H. Ding, K. S. Yeo, Local radial basis function-based differential quadrature method and its application to solve two-dimensional incompressible Navier-Stokes equations, Comput. Meth. Appl. Mech. Engrg. 192 (2003) 941–954.

[66] G. B. Wright, B. Fornberg, Scattered node compact finite difference-type formulas generated from radial basis functions, J. Comput. Phys. 212 (2006) 99–123.

[67] S. M. Wong, Y. C. Hon, T. S. Li, S. L. Chung, E. J. Kansa, Multizone decomposition for simulation of time-dependent problems using the multiquadric scheme, Comp. Math. Appl. 37 (1999) 23–43.

[68] J. Li, Y. C. Hon, Domain decomposition for radial basis meshless methods, Num. Meth. PDEs 20 (2004) 450–462.

[69] L. L. Ling, E. J. Kansa, Preconditioning for radial basis functions with domain decomposition methods, Math. Comp. Model. 40 (2004) 1413–1427.

[70] X. Zhou, Y. C. Hon, J. Li, Overlapping domain decomposition method by radial basis functions, Appl. Numer. Math. 44 (2003) 241–255.